Canadian Conference - Pacific Conference on Earthquake Engineering 2023
Vancouver, British Columbia
June 25th – June 30th, 2023

Topographic Amplification Factors For Different Potential Sliding Masses On A Rockfill Dam

Eric Krumm[1*] and Saman Zarnani[2]

[1]Geotechnical Engineer, BGC Engineering, Chile
[2]Principal Geotechnical Engineer, BGC Engineering, Canada
*ekrumm@bgcengineering.ca (Corresponding author)

ABSTRACT

Ground shaking during earthquakes can be affected by local site conditions, which can be separated into two components: soil amplification, due to amplifying or de-amplifying of seismic waves as they pass through the soil, from bedrock to ground surface; and topographic amplification, which refers to the interaction of seismic waves due to the 2D or 3D geometry where the waves travel through. Simplified semi-empirical correlations for estimating permanent seismic displacement during earthquake-induced deviatoric deformations using stick-slip models (e.g., Bray and Travasarou 2007, Bray et al. 2018 and Bray and Macedo 2019), use a 1D nonlinear fully coupled stick-slip sliding block. The seismic response of the sliding block is captured by an equivalent-linear viscoelastic modal analysis that uses strain-dependent material properties to capture the nonlinear response of the materials. In this way the soil amplification component of the total amplification is captured in the semi-empirical correlation. However, these 1D models can underestimate the seismic demand for shallow sliding masses at the top of 2D systems.

The objective of this study is to determine topographic amplification factors for the geometry of a rockfill dam for different potential sliding masses, to be used in semi-empirical correlations for seismic displacements using stick-slip models. To quantify the soil amplification, 1D soil columns were created in FLAC mirroring the geometry and stress distribution approximately along the highest dam portion. Following a similar process as Rathje and Bray (2001), a procedure is used for scaling 1D results to account for 2D topographic amplification and averaging of accelerations along different potential sliding masses on a rockfill dam. The results from the 1D columns are then compared to the 2D FLAC results to isolate the topographic amplification. Results were benchmarked to case histories and show that for shallow sliding masses, topographic amplification factors of up to 1.8 are expected.

Keywords: Topographic amplification, seismic displacement, rockfill dam, FLAC.

INTRODUCTION

Ground shaking during earthquakes can be affected by local site conditions, mainly referring to the thickness and stiffness of the soil layers present at site, from bedrock to ground surface. Accelerograms recorded in the last four decades have revealed in many cases that the subsurface characteristics can influence the acceleration amplitude level, the frequency composition, and the duration of shaking. The term "soil amplification" has been coined to describe the "filtering" which seismic waves undergo as they pass through the soil, and which tends to reinforce certain harmonic components of the incoming waves from the bedrock. On the other hand, soil "filtering" can also depress those harmonic components of the incident seismic wave whose frequencies exceed substantially the natural frequencies of the soil deposit and thus "de-amplification" of the shaking can be possible (Assimaki and Gazetas, 2004).

The presence of a topographic relief (such as a hill, a ridge, a canyon, a cliff, a slope, or the geometry of a dam or an embankment) can also influence the intensity and frequency composition of ground shaking during earthquakes. Such cases can also generate large amplification of ground shaking over short distances due to topographic effects. This phenomenon is more complicated to analyze than is "soil amplification" and can be very site specific, due to its truly two- or three-dimensional nature.

Figure 1 illustrates a simple 2D slope geometry. The site response can be represented by the maximum horizontal acceleration at various locations: the maximum free-field acceleration further away from the toe (a_{FF_t}), the maximum free-field acceleration far behind the crest (a_{FF_c}), and the maximum crest acceleration (a_{crest}), as shown in Figure 1. Using those basic definitions, three measures of acceleration amplifications can be computed (Ashford and Sitar, 2002):

- Topographic amplification at the crest: the amplification of the free-field motion away from the crest, compared to crest acceleration. This topographic amplification is predominantly due to the geometry of the slope.
- Soil amplification: the amplification due to the differences in the soil columns properties and heights further away from the toe and far behind the crest.
- Apparent amplification at the crest: the total apparent amplification of the motion between the free-field motion further away from the toe and the crest (Ashford and Sitar, 1997).

As shown in Figure 1, the total apparent amplification is the product of the soil amplification and the topographic amplification and can be quantified if each of those components are known separately.

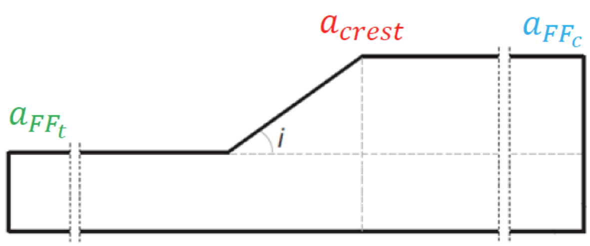

Topographic Amplification at the crest: $\dfrac{a_{crest}}{a_{FF_c}}$

Soil Amplification: $\dfrac{a_{FF_c}}{a_{FF_t}}$

Apparent Amplification at the crest: $\dfrac{a_{crest}}{a_{FF_t}}$

Apparent Amplification at the crest = Top. Amp x Soil Amp

$$\frac{a_{crest}}{a_{FF\,t}} = \frac{a_{crest}}{a_{FF_c}} \times \frac{a_{FF\,c}}{a_{FF\,t}}$$

Figure 1. Definition of different notations of amplification.

Bray and Travasarou (2007) (BT07) proposed a simplified semi-empirical correlation for estimating permanent seismic displacement during earthquake-induced deviatoric deformations. They used a 1D nonlinear fully coupled stick-slip sliding block. The seismic response of the sliding block was captured by an equivalent-linear viscoelastic modal analysis that used strain-dependent material properties to capture the nonlinear response of the earth materials. In this way the soil amplification component of the total amplification is captured in the semi-empirical correlation. The 1D model used by BT07 can underestimate the seismic demand for shallow sliding masses at the top of 2D systems where topographic amplification can be significant. To account for this, they recommended topographic amplification factors (TAF) of ~1.25 for moderately steep slopes (<60°) (based on Rathje and Bray, 2001) and ~1.5 for steep slopes (>60°) (based on Ashford and Sitar, 2002). This topographic amplification factor is applied as a multiplier to the spectral acceleration (Sa) that is used for calculating seismic displacement for a particular slip surface. The BT07 recommended amplification factors however those were developed for flat-topped slopes; California coastal cliffs in the case of Ashford and Sitar, and municipal solid waste piles in the case of Rathje and Bray. These slope configurations may not capture all the topographic amplification produced by the trapezoidal section geometry of an earth/rockfill dam.

Research by investigators (e.g., Bray and Rathje, 1998) has found that seismic displacements depend on the dynamic response characteristics of the potential sliding mass. The objective of this paper is to determine a topographic amplification factor for the geometry of an anonymous tailings embankment dam for different potential sliding masses TAF_{PSM}, to be used in Bray and Travasarou type correlations for estimating seismic displacements (Bray and Travasarou type correlations already include soil amplification by using stick-slip sliding block model). Following a similar process as Rathje and Bray (2001), a procedure is used for scaling 1D results to account for 2D topographic amplification and averaging of accelerations along different potential sliding masses. With the methodology presented herein the calculated TAF_{PSM} is only due to the two-dimensional dam geometry, not containing the soil amplification part. The computed TAF_{PSM} can be directly used in estimating seismic displacements using the BT07 (or similar) method for any desired potential sliding mass, for this specific tailings dam geometry.

ANALYSIS METHODOLOGY

Seismic amplification of ground motion due to 2D geometry topographic effects for an anonymous earth embankment tailings dam is investigated using computer software FLAC v8.0. FLAC (Fast Lagrangian Analysis of Continua, Itasca 2016) is a 2D explicit finite difference program that is commonly used to perform static and dynamic analyses of soil continuum problems.

The tailings dam is constructed using downstream construction method and has an upstream inclined core, supported by rockfill shells in the downstream and upstream. Three different intermediate dam construction stages (crest El. 182 m, El. 215 m and El. 245 m) plus the final dam crest (El. 258 m) models were simulated for this assessment. First, a static analysis was completed for each dam stage, using Mohr-Coulomb effective stress constitutive model with stress dependent strength and stiffness properties, to establish the static stresses prior to the seismic loading. Then a steady state seepage analysis was performed for each dam stage to establish the pore pressure conditions in the model. Then the constitutive models were switched to UBCSand-clay (for the core material, LPF) and UBCHyst (for all other dam fill material, e.g., rockfill and filters). Each case was brought into static equilibrium with these new constitutive models, prior to the application of the dynamic loading. A compliant base boundary condition was used at the bottom of the model (also called quiet or stress boundary). This boundary condition was applied only in X direction in the FLAC dynamic models. This boundary condition would not allow the downward propagating shear waves to be reflected back up into the model. The base boundary condition in the Y direction was kept as fixed velocity (i.e. rigid) to minimize the numerical issues related to base bending. The horizontal acceleration input motion was transformed into a stress time history and applied at the bottom boundary in the horizontal direction. A free-field boundary was applied to both left and right model boundaries to eliminate outward propagating wave energy returning to the model. To obtain the horizontal equivalent acceleration (HEA) of a potential sliding mass (to be discussed later), the entire X-acc time history was recorded at every gridpoint in the LPF core and the dam fills downstream of it.

To quantify the 2D topographic amplification it is required to isolate the soil amplification component of the response (see Fig. 1). To do this, a series of 1D columns were modelled for the different dam stages. 1D soil columns were also created in FLAC with a two-dimensional plane-strain grid represented by a stack of rectangular soil element in the vertical direction. The results from these 1D column dynamic analyses would later be compared to the 2D dynamic results to isolate the topographic amplification effects. The locations of these 1D columns were selected to be approximately in the middle of the crest of the 2D models, to represent the maximum height of the model. The 1D column models were constructed using the same material properties as their 2D counterpart, all components of stresses and pore water pressure conditions for the selected 2D zones were extracted from the 2D models after the seepage analysis was finished and applied as an initial condition to the zones in the 1D columns. This ensures that the 1D column correctly represents the stress state and the soil behaviour of that particular 2D column of the dam during shaking.

Figure 2 shows the FLAC model geometry of the four sections analyzed and the corresponding location of the 1D columns associated with each case.

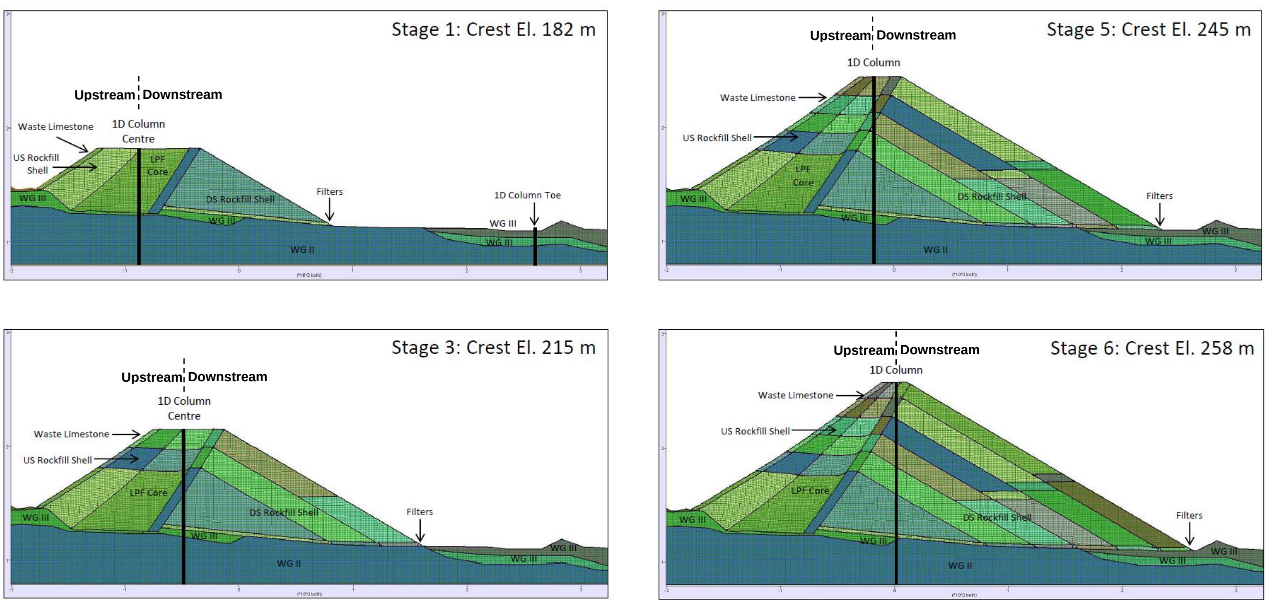

Figure 2. Dam stages and location of 1D columns analyzed.

Two earthquake motions were selected for use as input for the dynamic analyses in this assessment: Manjil (Manjil_Quzvin_LS_Hor) and Kocaeli (Kocaeli_Atakoy_LS_Hor) records (with adjusted PGA values of approximately 0.4g-0.5g). These two time histories were selected based on prior project work findings, which illustrated that these two records resulted in average estimated seismic displacements and the largest estimated seismic displacement, respectively, amongst other time histories used then. These two time histories were used for the dynamic analysis of all 1D columns and 2D dam stage models.

Ultimately, the TAFs were calculated for the two different ground motions at four different dam heights (or Stages) and several potential sliding masses (defined by different hypothetical slip surfaces). The next section describes in more detail the steps involved in the calculation of TAFs.

DETERMINATION OF TOPOGRAPHIC AMPLIFICATION FACTOR FOR A POTENTIAL SLIDING MASS

After all the 1D and 2D dynamic FLAC analyses described in the previous section were completed, the acceleration outputs were compiled and post processed. The topographic amplification factor for a potential sliding mass (TAF_{PSM}) is obtained after performing a three-step process:

- Step 1: The topographic amplification factor at the crest of the dam (TAF) is calculated as the ratio between the maximum horizontal acceleration at the crest (MHA_{2d}) and the maximum acceleration at the top of the corresponding 1D column (MHA_{1d}), using equivalent gridpoints (TAF= MHA_{2d}/ MHA_{1d}). Since the soil properties and the stress state are very similar between the 1D soil column and the corresponding area of the 2D model, the difference in acceleration response between the two models (1D vs 2D) is mainly attributed to the 2D topographic effects present at the 2D dam model (i.e., the soil amplification component in the two cases is very similar).
- Step 2: This step is to quantify how the topographic amplification at the crest (calculated in Step 1) changes with depth. Commonly, the seismic motion gets amplified closer to the top of the dam and near the surface due to focusing of the seismic waves and the doubling effect of the free surface. Deeper into the dam shell the topographic amplification tends to decrease due to incoherence and so a potential sliding mass would have an overall acceleration somewhat less than at the crest. To determine the TAF_{PSM}, the maximum horizontal equivalent acceleration at the crest ($MHEA_{crest}$) is calculated and compared with the maximum horizontal equivalent acceleration at the base of the potential sliding mass ($MHEA_{base}$). The calculation of horizontal equivalent acceleration at the crest and at the base of a potential sliding mass is explained in more detail in the following subsections.
- Step 3: The product of the above two steps is calculated to be the topographic amplification factor of that potential sliding mass, TAF_{PSM} (TAF_{PSM} = [TAF from Step 1] × [$MHEA_{base}$/$MHEA_{crest}$ from Step 2]).

Step 1 – Topographic Amplification at the Crest

The TAF is computed as the ratio between the maximum horizontal acceleration at the crest of the 2D model (MHA_{2d}) and the maximum horizontal acceleration at the top of the 1D model (MHA_{1d}). The gridpoint used in the 2D model corresponds to the equivalent gridpoint in the 1D model and is located at the bottom part of the top FLAC zone (i.e., second gridpoint from the top). This gridpoint was selected to be more representative since the most top gridpoint may have some non-realistic, high frequency acceleration response due to near zero confinement. This process is done for both seismic earthquake inputs and for every dam Stage. The recorded maximum horizontal accelerations at the top of the 2D and 1D models along with the calculated TAF are presented in Table 1. These maximum horizontal accelerations may occur at different instances of time in the 2D and 1D models. Figure 3a shows the TAF in graphical form as a function of dam height (measured from the foundation boundary to the crest of the dam at the dam centreline location). There is large scatter in the data, however, with a clear increasing trend in the TAF with dam height. A red dashed regression line is obtained as the result of Step 1 and represents the topographic amplification of the seismic input at the crest of the dam geometry. For short dam heights, minimal 2D effects would occur and the TAF should approach a value of 1.0 for a *zero height* dam.

Table 1. Topographic Amplification Factor at the dam crest measured as MHA_{2d}/MHA_{1d}

Model	Record	MHA_{2d} (1)	MHA_{1d} (1)	TAF = MHA_{2d}/MHA_{1d} (2)
Stage 1	Kocaeli	1.35	0.74	1.81
	Manjil	1.78	0.88	2.03
Stage 3	Kocaeli	1.68	0.70	2.38
	Manjil	2.14	1.17	1.83
Stage 5	Kocaeli	2.44	1.00	2.45
	Manjil	1.69	0.96	1.76
Ultimate	Kocaeli	1.52	0.97	1.58
	Manjil	2.16	0.87	2.50

Notes:
1. Accelerations measured in units of g. 1 g = 9.81 m/s^2.
2. Values in the table are rounded to 2 significant digits. Dividing directly from the table may not give the same results due to rounding errors.

Step 2 – Seismic Loading at the Base of the Potential Sliding Mass

During shaking, incoherence of seismic waves results in parts of a slope or a 2D dam geometry experiencing an acceleration in one direction, while other parts are accelerating in the opposite direction (Rathje and Bray, 2001). This incoherence is a result of a systematic wave passage effect as the predominantly vertically propagating shear waves travel up in the dam and interact with diffracted and reflected waves coming down or from the side slopes and down from the crest.

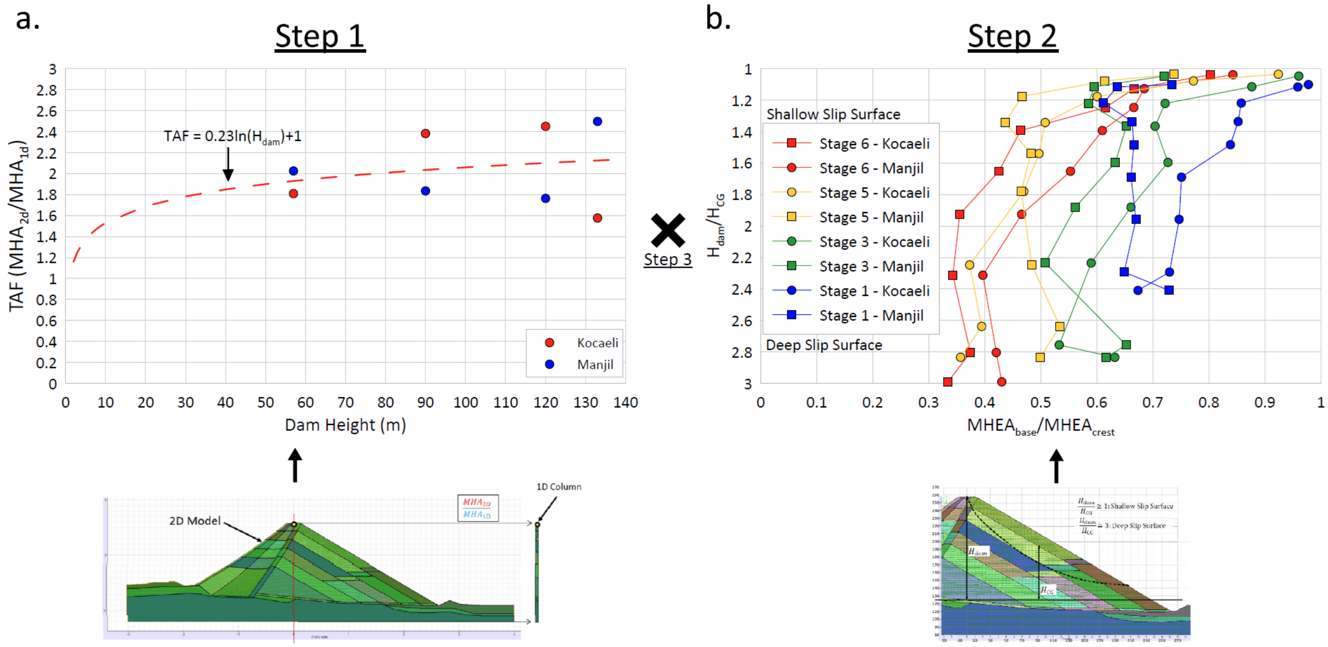

Figure 3. Steps 1 and 2 in the determination of the topographic amplification factor.

In the 2D models the maximum horizontal acceleration at the crest may only occur in one point along the crest surface of the dam. Accelerations vary along the dam crest, height, slope and into the dam fills due to the incoherence effects described above, hence the seismic loading on a potential sliding mass depends on its depth and length. To quantify how the acceleration response varies with depth and length of potential sliding masses, nine potential sliding masses were considered for each dam stage (Figure 4, defined by the hypothetical slip surfaces S1-S9). All the hypothetical slip surfaces were considered to commence at the upstream edge of the LPF core at the crest, regardless of their length or depth. This would allow to have the same horizontal equivalent acceleration at the crest (HEA_{crest}) for each potential sliding mass. To obtain HEAcrest, all the gridpoints at the base of the top-most elements, from the upstream edge of the LPF core to the downstream edge of the crest, are selected and the horizontal acceleration of those gridpoints were averaged in the time domain to produce an equivalent acceleration record.

The intent of the present work is to use the topographic amplification factors along with the Bray and Travasarou type seismic displacement calculation method. BT07 used a 1D nonlinear fully coupled stick-slip sliding block to perform their analysis with the seismic demand applied at the base of that sliding block. Similarly, in the present study, to account for the seismic demand at each PSM, the seismic demand is calculated along hypothetical sliding surfaces that define the base of the PSM. To calculate the horizontal equivalent acceleration at the base of each potential sliding mass (HEA_{base}), first the closest gridpoints to its base were selected. The horizontal acceleration of those gridpoints were then averaged in the time domain to produce an equivalent acceleration record. The HEA_{base} represents the seismic loading acting on the potential sliding mass that incorporates the incoherent nature of the seismic waves at the base of the slip surfaces. The maximum horizontal equivalent acceleration (MHEA) for the crest and for the base of different potential sliding masses analyzed with the two input motions are presented in Table 2.

The ratio of $MHEA_{base}/MHEA_{crest}$ is then calculated (values are shown in brackets in Table 2) to illustrate how the *average* acceleration response along the base of a potential sliding mass changes with depth, compared to the *average* acceleration response at the crest. In order to present these data in a normalized manner for all the analyzed cases and slip surfaces, the inverse of the centre of gravity (CG) of a potential sliding mass normalized by the dam height (measured from the top of the rock foundation) was used, as defined in Figure 5. The height of the CG of the different potential sliding masses considered, and defined by slip surfaces S1-S9 is presented in Table 3. Figure 3b illustrates the variation of $MHEA_{base}/MHEA_{crest}$ ratio against the potential sliding mass normalized height of the centre of gravity (decreasing trend of this calculated ratio with increasing normalized depth). These results indicate that the maximum equivalent acceleration for the entire sliding mass ($MHEA_{base}$) is smaller than the maximum equivalent acceleration at the crest of the slope ($MHEA_{crest}$). As the potential sliding mass gets deeper and larger, the length over which the accelerations are averaged is increased and the amplitude of the $MHEA_{base}$ decreases, due to incoherence of the waves.

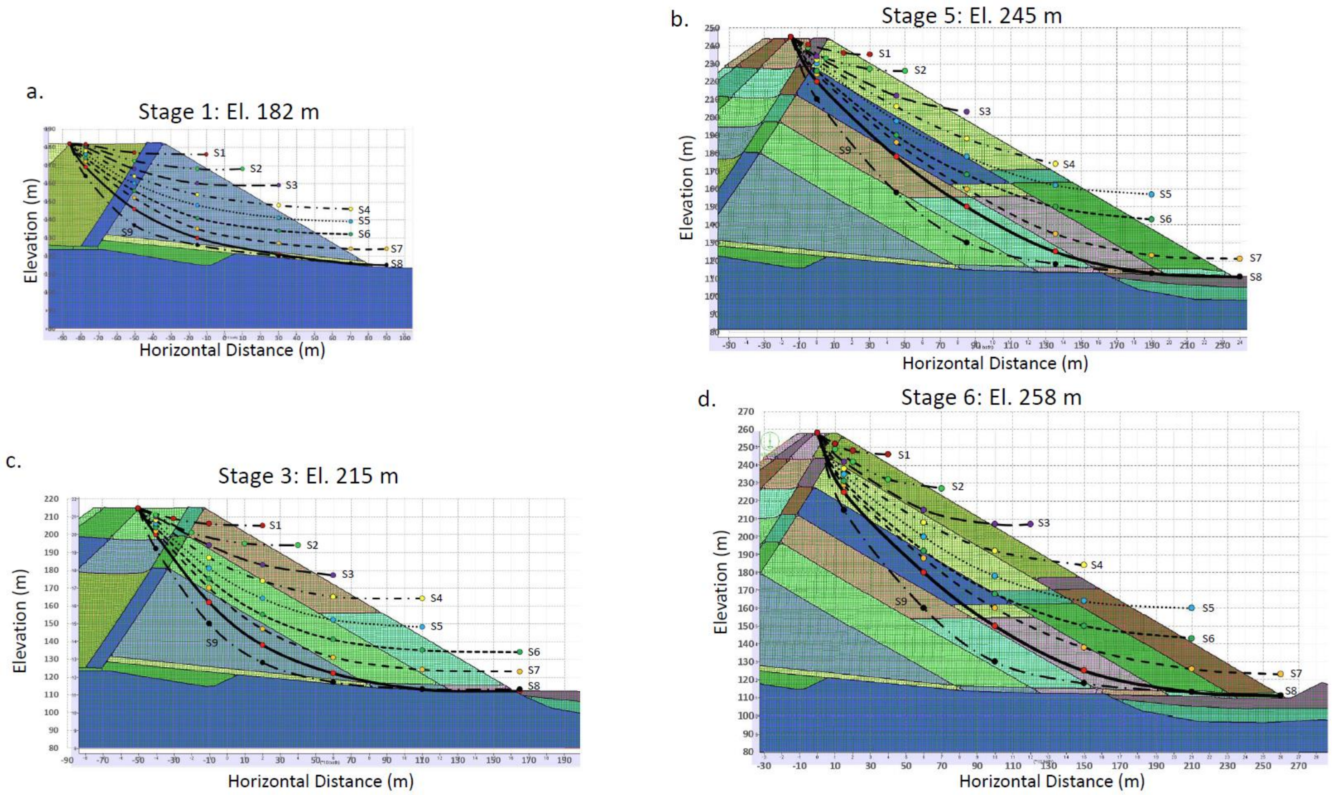

Figure 4. Potential sliding masses defined by slip surfaces 1 to 9.

Table 2. MHEA for different potential sliding masses

Model (H_{dam})	**Record**	**$MHEA_{base}$ at the base of the Potential Sliding Mass (1) (2) [ratio $MHEA_{base}/MHEA_{crest}$ shown in brackets] (3)**									**$MHEA_{crest}$ at the crest of the dam (1) (4)**
		S1	**S2**	**S3**	**S4**	**S5**	**S6**	**S7**	**S8**	**S9**	
Stage 1 (57 m)	Kocaeli	0.53 [0.98]	0.52 [0.96]	0.46 [0.86]	0.46 [0.85]	0.45 [0.84]	0.40 [0.75]	0.40 [0.75]	0.39 [0.73]	0.36 [0.67]	0.54
	Manjil	0.45 [0.73]	0.39 [0.64]	0.37 [0.61]	0.41 [0.66]	0.41 [0.67]	0.40 [0.66]	0.41 [0.67]	0.40 [0.65]	0.45 [0.73]	0.61
Stage 3 (90 m)	Kocaeli	0.63 [0.96]	0.57 [0.88]	0.47 [0.72]	0.46 [0.70]	0.48 [0.73]	0.43 [0.66]	0.39 [0.59]	0.35 [0.53]	0.41 [0.63]	0.65
	Manjil	0.52 [0.72]	0.43 [0.60]	0.43 [0.58]	0.48 [0.65]	0.46 [0.63]	0.41 [0.56]	0.37 [0.51]	0.48 [0.65]	0.45 [0.62]	0.73
Stage 5 (120 m)	Kocaeli	0.76 [0.92]	0.63 [0.77]	0.49 [0.60]	0.42 [0.51]	0.41 [0.50]	0.39 [0.47]	0.31 [0.37]	0.32 [0.39]	0.29 [0.36]	0.82
	Manjil	0.67 [0.74]	0.56 [0.61]	0.42 [0.47]	0.40 [0.44]	0.44 [0.48]	0.42 [0.46]	0.44 [0.48]	0.49 [0.53]	0.45 [0.50]	0.91
Ultimate (133 m)	Kocaeli	0.71 [0.80]	0.59 [0.67]	0.55 [0.62]	0.41 [0.46]	0.38 [0.42]	0.32 [0.36]	0.30 [0.34]	0.33 [0.37]	0.30 [0.33]	0.89
	Manjil	0.78 [0.84]	0.63 [0.68]	0.61 [0.67]	0.56 [0.61]	0.51 [0.55]	0.43 [0.47]	0.37 [0.40]	0.39 [0.42]	0.40 [0.43]	0.92

Notes:

1. Accelerations measured in units of g's. 1 g = 9.81 m/s^2.
2. At the base of each Potential Sliding Mass (defined by the hypothetical slip surfaces S1 to S9), the maximum acceleration of the equivalent record (i.e. the average record) of the gridpoints at the hypothetical slip surface is reported.
3. The ratio $MHEA_{base}$/ $MHEA_{crest}$ is shown in brackets.
4. At the crest of the dam, the maximum acceleration of the equivalent record (i.e. the average record) of the gridpoints located one row below the top of the crest nodes is reported.

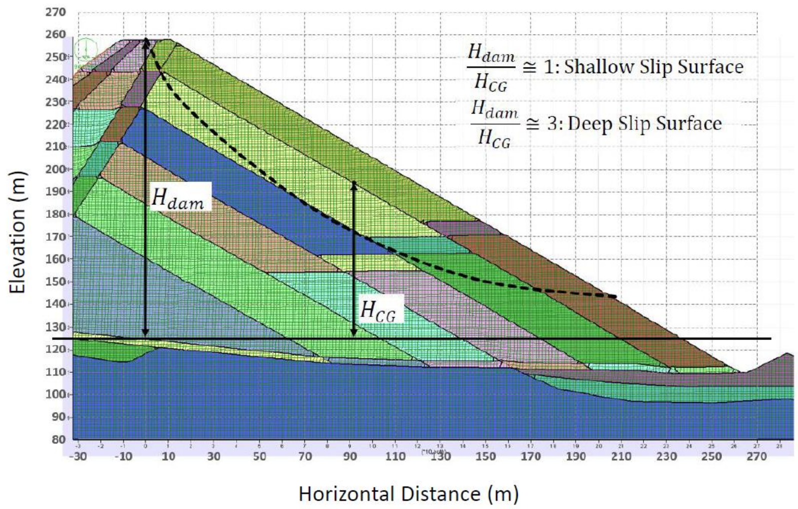

Figure 5. Definition of the potential sliding mass height normalization.

Table 3: Height of the centre of gravity (CG) for the different potential sliding masses.

Model	Dam Height (m)	H_{CG} (m) [(1)]								
		S1	**S2**	**S3**	**S4**	**S5**	**S6**	**S7**	**S8**	**S9**
Stage 1	57	52	51	47	43	38	34	29	25	24
Stage 3	90	86	81	74	66	56	48	40	33	32
Stage 5	120	116	111	102	89	78	67	53	46	42
Ultimate	133	128	118	107	96	81	69	58	47	45

Note:

1. The height of the centre of gravity (CG) for a potential sliding mass is measured from the base of the dam as indicated in Figure 5.

Step 3 – Topographic Amplification Factor of a Potential Sliding Mass

The TAF_{PSM} is calculated as the product of the amplification factors calculated from the regression line obtained from Step 1 and the $MHEA_{base}/MHEA_{crest}$ ratio for each potential sliding mass obtained from Step 2. The rationale for this step is that the calculated topographic amplification factor calculated at the top of the crest, does not exist in other parts of the dam fills and generally has to decrease with depth and the trends established from $MHEA_{base}/MHEA_{crest}$ ratios are used to account for that decrease for hypothetical slip surfaces deeper into the dam fills. The calculated TAF_{PSM} is illustrated in Figure 6. There is a large scatter in data, however, there is a trend in all the data as identified by a regression fit line for the entire data set using the computer program TableCurve2D®. Various mathematical relationships were investigated as candidates to best fit the data. A selected fit line of the form $x = a + b \cdot y^c$ was selected for this study due to its smooth transition, simple mathematical form and honoring the general trend in the data. The regression values determined are: a = 0.9911, b = 0.8274, and c = -4.12 as shown in Figure 6. In the above equation, x is the topographic amplification factor for a potential sliding mass (TAF_{PSM}), and y is the H_{dam}/H_{CG} ratio.

This equation can be used to estimate topographic amplification factors. These estimated topographic amplification factors can then be applied to the spectral acceleration values which are used in the calculation of Bray and Travasarou type displacements. For example; for the ultimate dam configuration (H_{dam} ~133 m) and the potential sliding mass with H_{dam}/H_{CG} of ~1.3, which means a hypothetical slip surface somewhere between S3 and S4 (Figure 4d), the estimated topographic amplification factor is ~1.25 (from Figure 6). This hypothetical slip surface is located in the upper half of the dam with a centre of gravity in the upper ~1/3rd of the dam height. The results from this assessment illustrate that the hypothetical slip surfaces located above this location (i.e. shallower slip surfaces) can have topographic amplification factors larger than 1.25 (and as high as ~1.8 for very shallow, surficial sloughing type slip surfaces close to the edge of the crest). On the other hand, it is expected that deeper hypothetical slip surfaces to have topographic amplification factors less than 1.25. The adopted correlation illustrates that for the maximum dam height, potential sliding masses with centre of gravity below the ~55% of dam height (i.e., $H_{dam}/H_{CG} > 1.9$), there is no considerable topographic amplification factor ($TAF_{PSM} < 1.05$), mainly due to the incoherence of the seismic motion discussed previously.

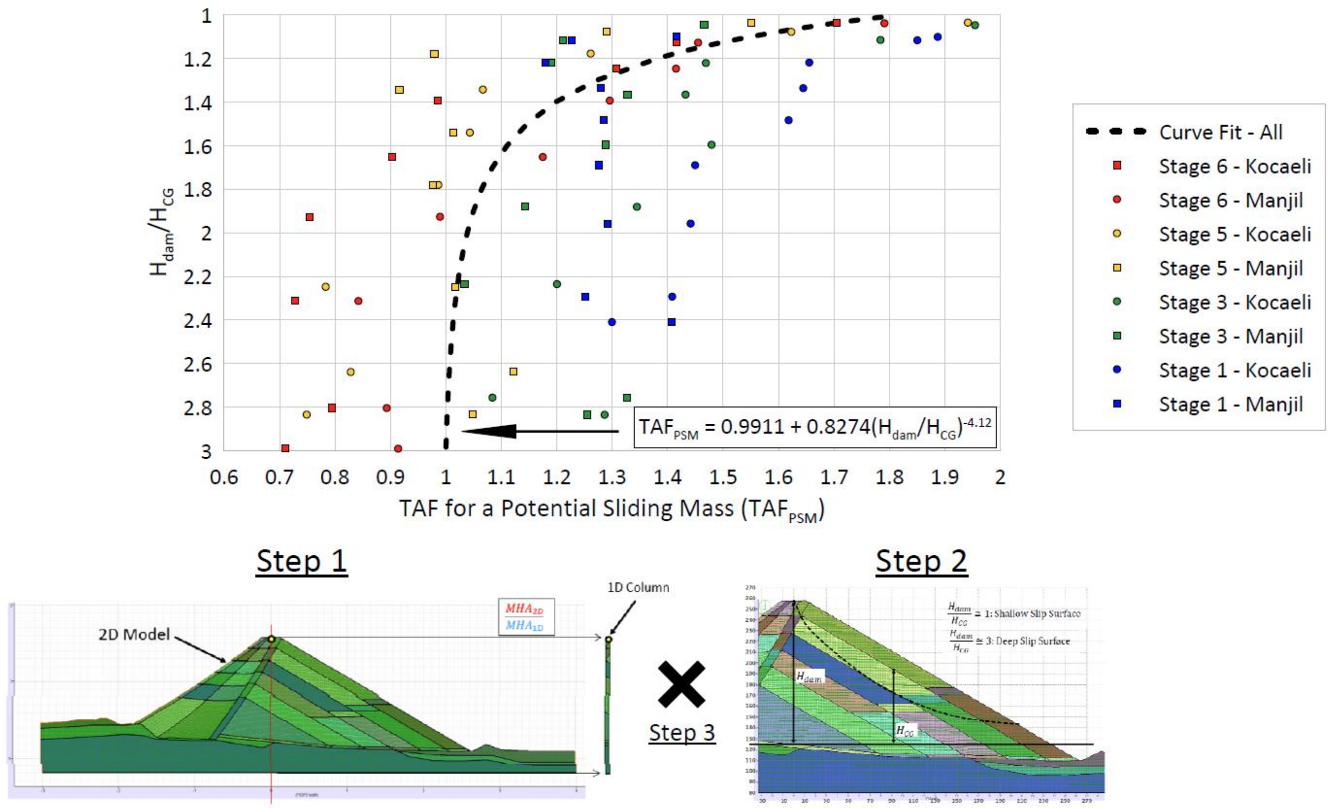

Figure 6. Final topographic amplification factor for a potential sliding mass.

BENCHMARKING

Yu et al. (2012) performed an extensive review of case histories of earth and rockfill dam behaviour during earthquakes. The peak crest accelerations and peak ground accelerations from 43 case histories were summarized. Results from finite element analysis of 6 typical dam cross sections and 12 real projects of modern high rockfill dams were also presented. The data set was divided in two categories: earth rockfill dams constructed before 1968 and modern well-compacted earth rockfill dams (constructed after 1968). They reported an 'acceleration amplified factor' that is interpreted as equivalent to the apparent amplification factor discussed in the Introduction section (Figure 1). Figure 7 shows the variation of the measured apparent amplification factor at the crest, from case histories. The data was obtained from real acceleration measurements during earthquakes and is presented for different dam categories as a function of PGA. The analyzed tailings dam in this study falls into Category B for modern well-compacted rockfill dams with heights larger than 75 m. Also superimposed on Figure 7 is the calculated apparent amplification factors from the upper bound curve proposed by Harder (1991) from the observed performance of earth dams during the Loma Prieta earthquake. This figure illustrates that Harder (1991) curve is within the range of the data presented by Yu et al. (2012).

The calculated soil amplification factor (Figure 1) falls in the range of approximately 1.1 to 1.3, by comparing the acceleration at the top of 1D FLAC columns (for the ultimate dam) and at the toe of the dam. The topographic amplification factor at the crest for the ultimate dam (H = 133 m) is equal to 2.12 according to Figure 3a. The apparent amplification is calculated as the product of these two factors and falls in the range of 2.3 to 2.8. This range is shown with blue dash lines on Figure 7.

Figure 8 shows the apparent amplification factor as a function of PGA from numerical analysis results of modern well-compacted rockfill dams. The apparent amplification factor from analyses by Yu et al. (2012) is shown both at the crest of the dam and also at the upper 1/5th of the dam. The TAF_{PSM_2} for Slip 2 for the ultimate dam is estimated to be ~1.5 (Figure 6). Then, the apparent amplification for the potential sliding mass defined by Slip 2 falls in the range of 1.5 to 1.8.

Both of these calculated ranges of amplifications from this study are in line with the historical data collected by Harder (1991) and Yu et al. (2012). This is an indication that the approach followed for this work, and the modelling results are consistent with actual seismic amplification in dams from real earthquake case histories.

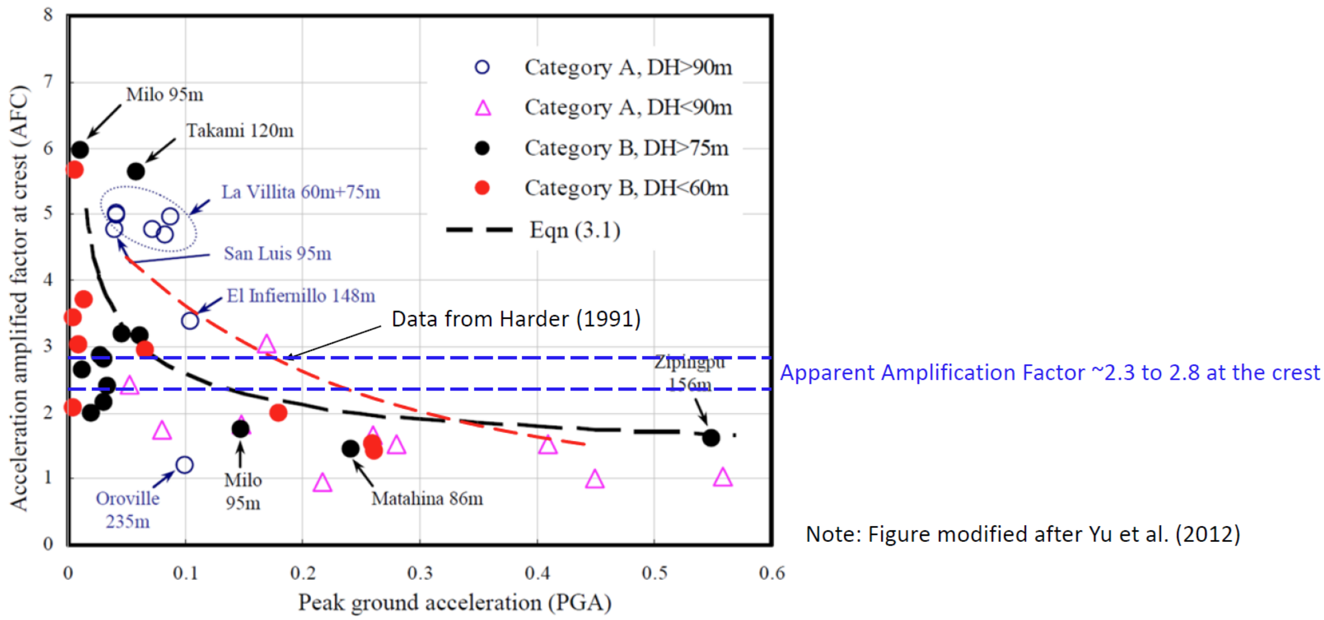

Figure 7. Benchmark of the apparent amplification at the modelled tailings dam to case histories.

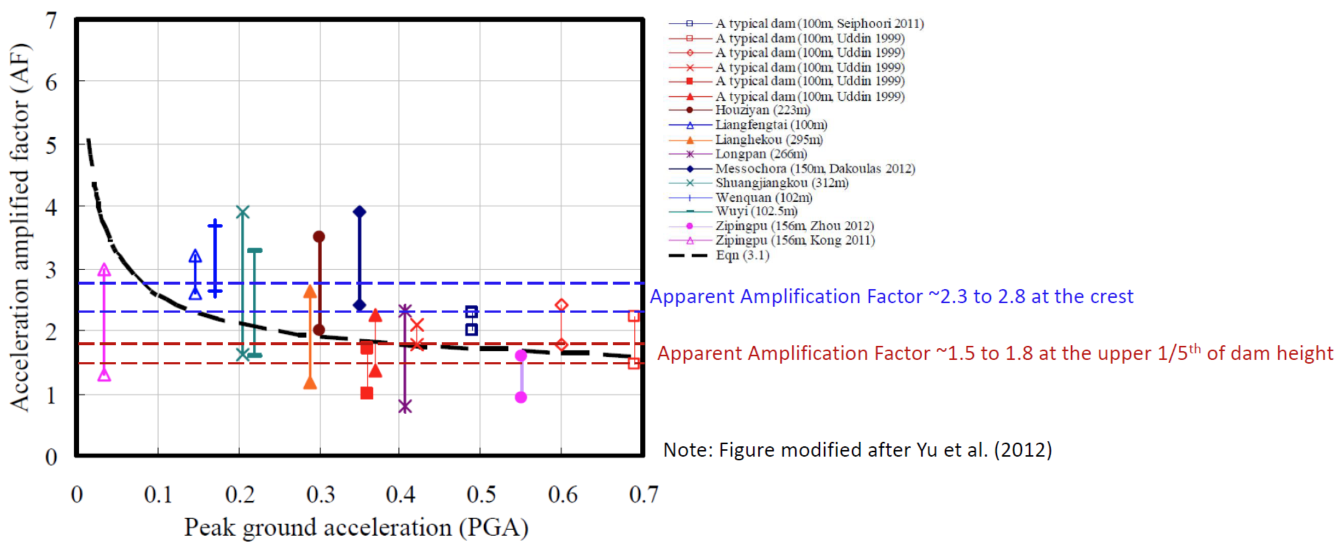

Figure 8. Benchmark of the apparent amplification at the modelled tailings dam to numerical models at other sites.

SUMMARY AND CONCLUSIONS

This paper presents a methodology and results for quantifying topographic amplification factor for an earth embankment tailings dam. These types of topographic amplification factors are required if seismic displacements are calculated using simplified methods such as Newmark's method or stick-slip models. The approach used in this paper, utilizes acceleration data from FLAC dynamic models for a two-dimensional dam geometry and also one-dimensional columns representing the middle of the dam. The topographic amplification factor is then calculated for the crest using this data. Then that crest topographic amplification factor is reduced for other hypothetical slip surfaces that are below the crest, accounting for the incoherence of acceleration response along the base of the slip surfaces. The data and the equation presented in Figure 6 can be used to estimate a "simplified" topographic amplification factor to be applied to the spectral acceleration values for use in stick-slip model type seismic displacement correlations. This simplified factor can account for 2D effects (topographic amplification) in a potential sliding mass for a 2D geometry and dam zonation properties similar to those of the simulated tailings dam in this study. The results show that for potential sliding masses with a ratio of H_{dam}/H_{CG} larger than ~1.9, no topographic amplification factor is required. The results show that the topographic amplification factor of 1.25 is reasonable for shallow slip surfaces, but values up to 1.8 can be expected for very shallow hypothetical slip surfaces. These topographic amplification factors can be multiplied to spectral acceleration values for use in Bray and Travasarou type seismic displacement correlations.

REFERENCES

[1] Assimaki, D. & Gazetas, G. (2004). Soil and topographic amplification on canyon banks and the 1999 Athens earthquake. *Journal of earthquake engineering: 8*(1), 1-43.

[2] Ashford, S. A., & Sitar, N. (2002). Simplified method for evaluating seismic stability of steep slopes. *Journal of geotechnical and geoenvironmental engineering 128*(2), 119-128. https://doi.org/10.1061/(ASCE)1090-0241(2002)

[3] Ashford, S. A., & Sitar, N. (1997). Analysis of topographic amplification of inclined shear waves in a steep coastal bluff. *Bulletin of Seismological Society of America*, 87(3), 692-700.

[4] Bray, J. D., & Travasarou, T. (2007). Simplified procedure for estimating earthquake-induced deviatoric slope displacements. *Journal of geotechnical and geoenvironmental engineering*, *133*(4), 381-392. https://doi.org/10.1061/(ASCE)GT.1943-5606.0000012, 1336-1340.

[5] Bray, J.D., Macedo, J., & Travasarou, T. (2018). Simplified Procedure for Estimating Seismic Slope Displacements for Subduction Zone Earthquakes. ASCE Journal of Geotechnical and Geoenvironmental Engineering, 144(3): 04017124

[6] Bray, J.D. & Macedo, J. (2019). Procedure for Estimating Shear-Induced Seismic Slope Displacement for Shallow Crustal Earthquakes, ASCE Journal of Geotechnical and Geoenvironmental Engineering. 145(12): 04019106.

[7] Rathje, E. M., & Bray, J. D. (2001). One- and two-dimensional seismic analysis of solid-waste landfills. *Canadian Geotechnical Journal*, *38*(4), 850-862.

[8] Bray, J. D., and Rathje, E. R. (1998). "Earthquake-induced displacements of solid-waste landfills." Journal of geotechnical and geoenvironmental engineering. 10.1061/(ASCE)1090-0241(1998)124:3(242), 242-253.

[9] Itasca (2016). FLAC – Fast Lagrangian Analysis of Continua, v8.0, Itasca Consulting Group Inc.

[10] Yu, L., Kong, X., & Xu, B. (2012). Seismic response characteristics of earth and rockfill dams. In Proceedings of the 15th World Conference on Earthquake Engineering, Lisbon, Portugal. September 2012. Paper ID (Vol. 2563).

[11] Harder, L. F. Jr. (1991). Performance of Earth Dams during the Loma Prieta Earthquake. *International Conferences on Recent Advances in Geotechnical Engineering and Soil Dynamics.* 11. https://scholarsmine.mst.edu/icrageesd/02icrageesd/session12/11